

# Statistical Analysis of Outer Electron Radiation Belt Dropouts: Geosynchronous and Low Earth Orbit Responses During Stream Interfaces

Olakunle Ogunjobi<sup>1</sup>, Andrew. B. Collier<sup>1,2</sup> and Craig J. Rodger<sup>3</sup>

<sup>1</sup>School of Physics, University of KwaZulu-Natal, Private Bag X54001, Durban 4000, South Africa

<sup>2</sup>SANSA Space Science, P. O. Box 32, Hermanus 7200, South Africa

<sup>3</sup>Department of Physics, University of Otago, Dunedin 9054, New Zealand

E-mail: olakunle.ukzn@gmail.com

**Abstract.** The OMNI-2 data set enables a correlation study of solar wind and geomagnetic parameters, allowing the stream Interfaces events (SIs) to be examined. A superposed epoch analysis of these events was performed to determine the threshold levels of IMF Bz and other geophysical parameters. Based on energy, temporal and spatial characteristics, statistical analysis of electron flux data from LANL-SOPA and NOAA- POES satellites were used to study outer zone electron dropouts and precipitation. The deepest minimum of electron flux was observed after the impact of a SI, which coincided with the time of slower-decaying peak of electron precipitation. Results suggest that the mechanism causing the precipitation could also be responsible for the observed electron flux dropout during Stream Interference.

## 1. Introduction

Earth's magnetic field traps energetic particles in the radiation belts. The radiation belts consist of an inner belt ( $1.1 < L < 2.5$ ), an outer belt ( $3 < L < 9$ ), and an intermediate region with depleted energetic fluxes known as the slot-region ( $2.5 < L < 3.0$ ). The outer radiation belt, is highly dynamic, with daily changes in electron flux. Without violation of any of the three adiabatic invariants, trapped radiation-belt particles would indefinitely undergo three types of periodic motion: gyration, mirroring between the northern and southern hemispheres, and drift motion. The loss processes in outer radiation belt have become a topic of interest over the last decades; yet the principal mechanism depopulating this belt is unknown [1]. However, it has been recently shown that the outer radiation belt's energetic particle fluxes can undergo dramatic temporal variations as response to stream interface events (SIs). The bimodal structure of solar wind, that is, two basic populations: slow and fast provide the platform for SI occurrence. The slow solar wind comes from the vicinity of streamer belt and always at the leading edge of the fast solar wind which originates from coronal holes. The region that separates dense, slow-moving plasma from fast, less dense plasma is a stream interface. The cleaned 66 subset of SI events identified by [2] are herein used in our statistical studies. One major characteristic of SI events on arrival at earth is the deflection of solar wind azimuthal velocity (GSE- $V_y$ ) as shown in figure 1 for the 66 events. In this paper, the focus is primarily on outer electron radiation belt dropouts due to SI at Geosynchronous Earth Orbit (GEO) and Low Earth Orbit (LEO). These orbits are

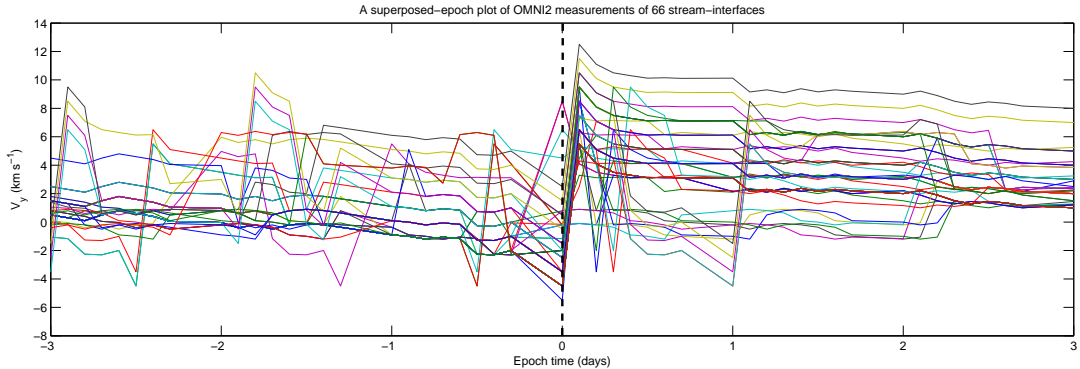


**Figure 1.** The Solar Wind Azimuthal Velocity (GSE- $V_y$ ) for each of the 66 SIs.

interesting regions for space weather applications as large numbers of spacecraft neighbouring there providing for magnetospheric and atmospheric processes. In the second session, the data set use as well as the the techniques employed in analysing the data is described. Third, the implication of the events are explored by analysing some geophysical parameters and solar wind conditions. Fourth, we analysed the statistical responses to dropouts during SI events at GEO. Fifth, the statistical relationship between trapped electron flux levels and degree of precipitation at LEO are also analysed and lastly, we conclude of on the varying statistical analyses.

## 2. Data description and Techniques

Using the events in [2], solar wind and geomagnetic parameters were obtained from Omni-2 data (<http://omniweb.gsfc.nasa.gov>). We cleaned the events by removing those with solar proton contamination before use. The energetic electron dropouts were measured using data from multispacecraft Synchronous Orbit Particle Analyser (LANL/SOPA) located at GEO with nominal data coverage of 24-hours daily. At every 10.24 seconds, SOPA instruments measure differential fluxes of electrons from 50keV to greater than 1.5 MeV in 12 channels. The SOPA telescopes are actively controlled such that the spin axis of the satellite points continuously toward the centre of the Earth. The SOPA flux measurement used here were from three electron channels (225-315 keV, 315-500 keV and 0.75-1.1 MeV) from the LANL spacecraft. For every operational spacecraft, flux data were normalised to obtained the same yearly averaged logarithm [3]. Thus, we have obtained logarithmic average by summation of log-fluxes divided by the number of satellites per time. Additionally, NOAA/POES (15-18) serve as proxy for wider range of L values and magnetic local time. The orbits of these satellites are polar and Sun-synchronous at an altitude of about 850 km and with a period of 100 minutes. The Medium Energy Proton and Electron Detector (MEPED) on each satellite provides directional ( $0^\circ$  telescopes for precipitating and  $90^\circ$  for trapped) measurements of energetic electrons but with proton contamination [4]. In order to reduce contamination, we applied first order correction suggested by [5]. The L used is from IGRF model for the event period. For clarity purpose, we present superposed average of  $> 30$  keV electron flux at  $0^\circ$  ( $90^\circ$ ) that is, precipitating (trapped) channels across three spatial cut (L= 4.02, 5.02 and 6.02) using POES 15 and 17 (2030-0630 MLT) and POES 16 and 18 (0730-1930 MLT). With POES satellites, our superposed epoch is organised across all MLT such that at any given MLT, one of the POES satellite provides coverage.

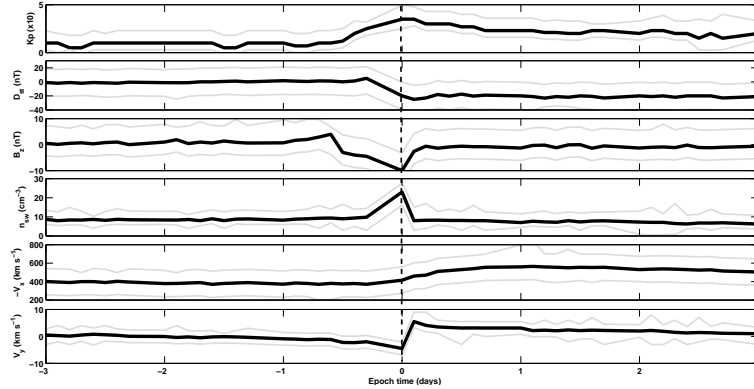


**Figure 2.** Plots of superposed properties of SIs used: in each panel the grey lines are the upper and lower percentiles while black line indicates the average, with the zero epoch taken as the time of  $V_y$  reversal. From top (first-sixth) is  $K_p$ ,  $Dst$  (nT), GSM  $B_z$  (nT), proton number density, solar wind radial velocity ( $-V_x$  GSE) and solar wind azimuthal velocity (GSE- $V_y$ )

For all acquired data, the reference time of our superposed epoch analysis is set to SI onset which is defined as reverse point from westward to eastward flow of solar wind azimuthal velocity. The data extracted at this reference time were 3-hourly averaged and for robustness, we also show the dispersion of geophysical parameters and equatorial electron flux observations by providing upper and lower percentiles at each time.

### 3. SIs: geophysical observations

Figure 2 presents various superposed geomagnetic and solar wind conditions around the time of SI used in our study. In Figure 2 (first panel), superposed average of  $K_p$  as a measure of magnetospheric convection is seen to be at peak of 3+ at approximately 3 hours after the arrival of SIs and returns to the pre event level in 0.5 day. Figure 2 (second panel), displays measurement of ring current,  $Dst$  (nT) shows positive value of about 15 nT prior to the arrival of SI indicating weakly magnetospheric convection pressure and reverses to storm of -30 nT at SI arrival implying small strengthened ring current.  $Dst$  perturbation continues through a day although at relatively low level as can be seen. Also in figure 2, third panel, is the superposed average of  $B_z$ - component (GSM coordinate) which prior to the arrival of SI was distinctly in Northward peak of 10 nT and reversed southward close to the arrival of SI. The threshold value of GSM- $B_z$  of less than -10 nT persists for about 3 hours at SI arrival. Figure 2 (fourth panel), shows the superposed plot of proton number density with sharp peak at the arrival of SI reaching approximately  $19 \text{ cm}^{-3}$  on averaged scale indicating difference of dynamic-pressure as fast wind overtakes slow wind. Prior to this abrupt increase, proton number density is found at relatively low level. The solar wind radial velocity (GSE  $-V_x$ ) is presented in figure 2 (fifth panel) showing greater than 300 km/s before SI arrival. Just at SI onset,  $-V_x$  is elevated to range of greater than 500 km/s for 3 days after SI implying that high-speed-stream driven storms last for several days. In Figure 2 (sixth) the GSE  $y$ -component (solar wind azimuthal velocity) is shown. Close to the day 0,  $V_y$  is at the level of around -9 km/sec on average but reverses to a point of approximately +10 km/s on average scale indicating arrival of SI at Earth. As can be seen, the  $V_y$  through 0.1 day maintains a steady flow at the passage of SI.

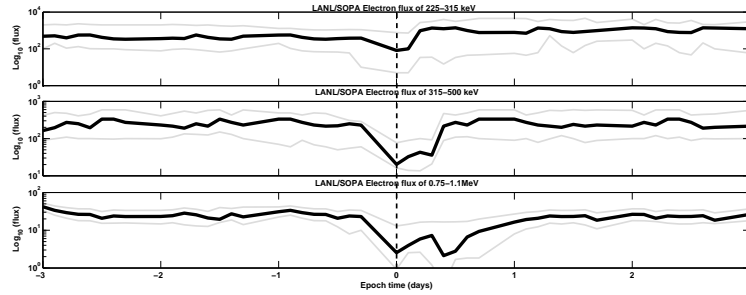


**Figure 3.** Superposed epoch plots of electron flux as measured by combined LANL SOPA and GOES satellites: (top) is 225 to 315 keV, (middle) is 315 to 500 keV, (bottom) is the 0.75 to 1.1 MeV and (fourth) is GOES  $> 2$  MeV. The dash vertical line indicates arrival of SI. Format is as in Figure 2.

#### 4. Equatorial Observation of Electron flux dropout

In this session, we present dropouts as measured from GEO. Observations at GEO can also be compared with global positioning system (GPS) taken at  $L^* = 4 - 4.5$  when considering adiabatic effects. It will be reasonable to say there is less mixing of adiabatic effects in our analyses since sets of SIs used here do not follow strong enhancement in ring current. Figure 2 presents an overview of superposed average of the logarithm of 225 - 315 keV, 315 - 500 keV and 0.75 - 1.1 MeV electron flux as measured by LANL/SOPA multiple satellites around GEO. In Figure 3 (top), electrons of 225 - 315 keV is plotted showing gradual dropout of electron flux from -1 (day) and drops to minimum at approximately 3 hours after the arrival of SI and recovers quickly to pre-event level in less than a day. In Figure 3 (middle) is the electron flux of 315 - 500 keV and as can be seen there is also gradual dropout prior the arrival of SI but electron flux dropout is about 0.78 magnitude deeper than in 225 - 315 keV channel at arrival of SI. The recovery is seen to be slightly higher than the pre-event level for more than three days. Figure 3 (bottom) shows electrons of 0.75 - 1.1 MeV, there is also observed gradual dropout from -0.5 day till 0.8 day after the arrival of SI. The dropout magnitude is seen to be about 1.55 and 0.11 order differ from 225 - 315 keV and 315-500 keV channel respectively while the recovery level is higher than pre-event level more than 3 days.

#### 5. Estimate of $> 30$ keV Electron Flux From LEO

Figure 4 displays POES  $> 30$  keV flux at L of 4.02, 5.02 and 6.02. In Figure 4 (top), electron flux at  $L= 4.02$  is plotted, as can be seen there is a gap of more than factor of 5 difference between trapped and precipitating flux preceding and few hours following the arrival of SI which indicates no substantial precipitation then. The narrow peak is seen on arrival of SI reaching about  $7 \times 10^3$  flux. Figure 4 (middle) is the plot of  $> 30$  KeV at  $L = 5.02$  with more than factor of 5 gap between trapped and precipitating flux preceding and a day following the SI implying bursty precipitation at this region. The peak with slower decaying character is observed in both trapped and precipitating electron flux at SI arrival. Also, as can be seen, precipitating flux of electron is about  $10 \times 10^5$  flux at SI arrival. Figure 4 (bottom) shows  $> 30$  keV electron flux at  $L= 6.02$  both trapped and precipitating electron flux showing systematic variation. Also, gap of more than factor of 5 is seen preceding and a day after SI indicating that bursty precipitation extended to this region. Precipitating electron flux as can be seen reaches about  $15 \times 10^4$  flux on SI arrival.

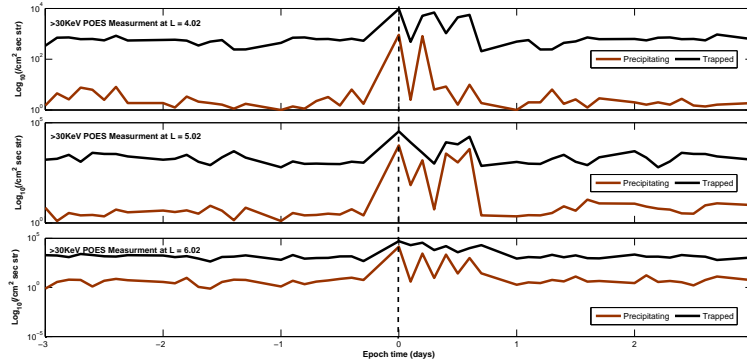


**Figure 4.** Superposed epoch plot of  $> 30$  keV electron flux measured by NOAA/POES (15-18) satellite. The black line in each plot indicates measurements from  $90^\circ$  telescope (trapped flux) while the red line indicates measurements from  $0^\circ$  telescope (precipitating flux). The dash vertical line indicates arrival of SI (top) is the  $>30$  KeV at  $L = 4.02$ , (middle) is  $L = 5.02$  while (bottom) is fluxes at  $L = 6.02$

Similar to  $L = 5.02$ , the simultaneous slower decaying peak of both trapped and precipitating electron flux began approximately 0800 MLT to around 1400 MLT on the time of SI as can be seen, there is almost same lower level variation generally maintained between 1500-0500 MLT.

## 6. Summary and Conclusion

Superposed epoch analysis shows that these set of event occurred during southward GSM-Bz. This confirms the compression of magnetosphere in slow solar wind [2] during the events.

Across GEO, there is tendency for outer electron radiation belt dropouts prior the arrival of SI but reaches deepest minimum mostly at 3 hours after arrival of SI. The recovery is also seen to be rapid at lower energies. This analysis corresponds to the Global Positioning System (GPS) observation of  $L^* = 4.5$  reported by [2], who found dropout to be energy and  $L^*$  dependent with combined radial diffusion and loss through magnetopause as the likely cause.

POES 15-18 orbiting LEO shows that more than 30 keV precipitating electron flux level is about factor of 5 lower than trapped flux preceding and about a day following the time of the event. Consistent with some previous observations, e.g [6, 5], there is tendency in precipitation following the trend of trapped flux. our statistical analysis revealed an unstructured abrupt peak (with slower decaying character) in precipitating electron flux on arrival of SI which coincided with time of deepest minimum of observed dropouts. Analysis also reveals  $L = 5.02$  and  $L = 6.02$  as region with higher precipitation of electron flux. These observations could be infer to explanation of some loss mechanisms under high speed stream-interference.

## Acknowledgments

We are thankful to the JPCS organizers, and especially Botha Roelf, for the invitation to present this work to this proceedings. We thank R. Friedel for providing LANL/SOPA data. Research was supported by the SANSa Space Science research program. We also thank providers of NOAA/POES data in NSSDC, and the OMNI-2 Data sets.

## References

- [1] Friedel R H W, Reeves G and Obara T 2002 *Journal of Atmospheric and Solar-Terrestrial Physics* **64** 265
- [2] Morley S K, Friedel R H W, Spanswick E L, Reeves G D, Steinberg J T, Koller J, Cayton T and Noveroske E 2010 *Proceedings of Royal Society* **466** 3329–3350

- [3] Belian R D, Gisler G, Cayton T and Christensen R 1992 *Journal of Geophysical Research* **97** 16897
- [4] Rodger C J, Clilverd M A, Green J C and Lam M M 2010 *Journal of Geophysical Research* **115** A04202
- [5] Lam M M, Horne R B, Meredith N P, Glauert S, Moffat-Griffin T and Green J C 2010 *Journal of Geophysical Research* **115** A00F08
- [6] Clilverd M A, Rodger C J, Gamble R J, Ulich T, Raita A, Seppälä A, Green J C, Thomson N R, Sauvaud J A and Parrot M 2010 *Journal of Geophysical Research* **115** A12304